ALTEX, accepted manuscript
published July 27, 2023
doi:10.14573/altex.2302011

Research Article

Intestinal *In Vitro* Transport Assay Combined with Physiologically Based Kinetic Modeling as a Tool to Predict Bile Acid Levels *In Vivo*

Véronique M. P. de Bruijn, Willem te Kronnie, Ivonne M. C. M. Rietjens and Hans Bouwmeester
Division of Toxicology, Wageningen University and Research, Wageningen, The Netherlands

Abstract
Bile acid homeostasis is vital for numerous metabolic and immune functions in humans. The enterohepatic circulation of bile acids is extremely efficient, with ~95% of the intestinal bile acids being reabsorbed. Disturbing intestinal bile acid uptake is expected to substantially affect intestinal and systemic bile acid levels. Here, we aimed to predict the effects of apical sodium-dependent bile acid transporter (ASBT)-inhibition on systemic plasma levels. For this, we combined the *in vitro* Caco-2 cell transport assays with physiologically based (PBK) modeling. For this proof-of-principle study we used the selective ASBT-inhibitor odevixibat (ODE) as a model compound. Caco-2 cells grown on culture inserts were used to obtain transport kinetic parameters of glycocholic acid (GCA). The apparent Michaelis Menten constant ($K_{m,app}$), apparent maximal intestinal transport rate ($V_{max,app}$) and ODE's inhibitory constant (K_i) were determined for GCA. These kinetic parameters were incorporated in a PBK model and used to predict the ASBT inhibition effects on plasma bile acid levels. GCA is transported over Caco-2 cells in an active and sodium-dependent manner, indicating the presence of functional ASBT. ODE inhibited GCA transport dose-dependently. The PBK model predicted that oral doses of ODE reduced conjugated bile acid levels in plasma. Our simulations match *in vivo* data and provide a first proof-of-principle for the incorporation of active intestinal bile acid uptake in a bile acid PBK model. This approach could in future be of use to predict the effects of other ASBT-inhibitors on plasma and intestinal bile acid levels.

1 Introduction

Bile acids (BAs) have emerged as critical signaling molecules for energy, glucose and lipid metabolism, cell proliferation as well as regulation of the immune system (Jia et al., 2018; Fuchs and Trauner, 2022). BA homeostasis is primarily regulated by the gut-liver axis, where primary BAs are produced in the liver, metabolized to more hydrophobic secondary BAs by the intestinal microbiome and taken up via the intestinal epithelium into the portal vein to be recirculated to the liver. The BA pool shapes the microbiome community by acting on bacterial cell membranes, but also reduces intestinal membrane integrity by affecting the epithelial cells (Begley et al., 2005). High amounts of the secondary BA deoxycholic acid (DCA) reduced intestinal integrity in pig colonic crypts (Leschelle et al., 2002) and in rabbit small intestine (Fasano et al., 1990). Reduced intestinal integrity is related to diarrhea, bacterial overgrowth and inflammatory bowel disease (Marasco et al., 2022; Miele et al., 2009). Furthermore, bacterial products are more likely to translocate to the liver and trigger an inflammatory response in case of reduced membrane integrity. Intestinal inflammation may then translocate to the liver, ultimately resulting in liver inflammation and stress responses (Duan et al., 2022; Sabino et al., 2016). Disturbances of the BA pool predisposes an individual to the development of liver disease, e.g., cholestasis (Gijbels and Vinken, 2019), Non-Alcoholic Fatty Liver Disease (NAFLD) (Mouzaki et al., 2016) and gastrointestinal carcinogenesis (Li et al., 2022). It has been shown that fecal concentrations of DCA and its conjugates increased with disease activity and fibrosis stage, an important hallmark of NAFLD (Smirnova et al., 2022). Hence, a well-balanced BA pool is essential for gut-liver axis homeostasis and human health.

BAs are *de novo* synthesized in the liver from cholesterol. Upon conjugation with glycine or taurine, BAs are actively secreted via the Bile Salt Export Pump (BSEP) to the bile canaliculi (Lin et al., 2023). Via the bile canaliculi, the conjugated BAs enter the intestinal lumen where they can be deconjugated and where ~95% of intestinal BAs is reabsorbed via both active and passive processes (Kullak-Ublick et al., 2004). Unconjugated BAs are passively absorbed along the whole length of the small intestine, while the majority of both conjugated and unconjugated BAs is actively reabsorbed from the ileum (Martinez-Augustin and Sanchez de Medina, 2008; Krag and Phillips, 1974; Li et al., 2018). The most effective reabsorption of BAs takes place in the terminal ileum and is mediated by the apical sodium-dependent bile acid transporter (ASBT), a member of the solute carrier (SLC) super-family encoded by the *SLC10A2* gene (Dawson, 2011; Lin et al., 2023). Via ASBT, BAs are taken up in the enterocytes where they bind to the Bile Acid Binding Protein (BABP) and are excreted to the basolateral side in the

Received February 1, 2023; Accepted July 25, 2023;
Epub July 27, 2023; © The Authors, 2023.

ALTEX 40(#), ###-###. doi:10.14573/altex.2302011

Correspondence: Véronique M. P. de Bruijn, PhD
Division of Toxicology
Wageningen University and Research
Wageningen, 6708 WE, The Netherlands

portal blood via the organic solute transporter (OST) α/β (Lu et al., 2022). Via the portal vein the BAs are transported to the liver where they are taken up by Na^+-taurocholate co-transporting polypeptide (NTCP) and transporters from the organic anion transporting polypeptide (OATP) family (Chiang and Ferrell, 2022). BAs that escape ileal reabsorption are metabolized by the gut microbiome into a wide array of secondary BAs, followed by either absorption from the colon or fecal excretion (Jia et al., 2018). The remarkably efficient uptake of BAs from the intestinal lumen implies that this process is of crucial importance for BA homeostasis, and alterations in intestinal BA uptake potentially affect the onset and development of different types of liver disease (Duan et al., 2022; Yang et al., 2020). Consequently, ASBT has been an attractive target for drug development since its discovery. For instance, odevixibat (ODE) has recently been approved for the treatment of progressive familial intrahepatic cholestasis, and trials for the treatment of other cholestatic diseases are still ongoing (Deeks, 2021). ODE is a selective and reversible ASBT-inhibitor, and the drug reduces the BA levels in plasma/serum by reducing the reuptake of BAs in the ileum, while the fecal BA levels are increased (Graffner et al., 2016). Individuals with progressive familial intrahepatic cholestasis typically have increased plasma BA levels, and a reduction is considered beneficial in these specific cases. Reduced bile acid absorption was observed in preclinical and clinical studies of inflammatory bowel disease, and was typically accompanied by decreased ASBT levels (Fitzpatrick and Jenabzadeh, 2020). This indicates that even though a reduction of ASBT-mediated BA absorption is beneficial for individuals suffering from cholestatic diseases, it might have an adverse effect on otherwise healthy individuals. Several xenobiotics, e.g., the mycotoxin deoxynivalenol and the antibiotic tobramycin, are known to reduce intestinal BA uptake *in vitro* (Wang et al., 2022; Zhang et al., 2022). For an accurate human hazard assessment of chemicals, it is crucial to understand how xenobiotics alter BA homeostasis and could potentially affect host health.

Quantitative knowledge of the synthesis, absorption, distribution, metabolism, and excretion of BAs is paramount for understanding BA-associated pathologies. Here, physiologically based kinetic (PBK) modeling provides a powerful tool to integrate physicochemical and biological properties of BAs, and to predict the effects of drug interventions or xenobiotic exposure without the need for animal derived data. PBK modeling contributes thus to the 3R principle (Replacement, Reduction and Refinement) in chemical risk assessment. Several kinetic models describing the processes involved in BA homeostasis have been developed previously. Early work describes the metabolism and circulation of several major BAs in the gastrointestinal tract and circulatory system (Hofmann et al., 1983; Molino et al., 1986). Active transport processes are increasingly being recognized as important modulators in the BA homeostasis, but they were not included in this early work. For example, inhibition of BSEP can lead to a toxic BA accumulation inside hepatocytes and cause cholestasis. The relevance of hepatic BSEP inhibition for cholestasis development has been recognized in the Cholestasis Adverse Outcome Pathway (AOP) (Vinken et al., 2013). Active transport processes were included in more recent modeling work (Sips et al., 2018; Voronova et al., 2020; Baier et al., 2019). Advancements in computational power and biological understanding of the processes involved in BA homeostasis allowed for the development of more complex and dynamic models. The work of Voronova et al (2020), for example, described the autoregulation of BA synthesis by farnesoid receptor X (FXR) (Voronova et al., 2020), and Sips et al. (2018) modelled the intestinal transit of BAs in detail (Sips et al., 2018). Increased complexity of mathematical models typically comes with an increased number of required input parameters – parameters that cannot always be derived experimentally and pose the risk of overfitting. Therefore, we previously developed a data-driven PBK model describing BA homeostasis, i.e., a PBK model with the vast majority of parameters derived experimentally. The model included active BSEP-mediated hepatic canalicular BA efflux (de Bruijn et al., 2022a), but did not yet include transporter-mediated hepatic sinusoidal BA uptake or ASBT-mediated ileal BA absorption. In the present study we aim to extend the PBK model to also include ASBT-mediated ileal BA absorption and NTCP-mediated hepatic uptake and predict the effects of ASBT-inhibition on systemic plasma levels. This provides mechanistic insights in the effects of ASBT and its inhibition on whole-body BA homeostasis, with a focus on the gut-liver axis. To this end, we employed PBK modeling, and we evaluated the effect of ODE-mediated ASBT-inhibition on plasma BA levels. The required kinetic parameters for ileal absorption were derived from human Caco-2 cells grown in culture inserts. We focused on the glycine-conjugated forms of three major bile acids, i.e., glycocholic (GCA), glycochenodeoxycholic (GCDCA) and glycodeoxycholic acid (GDCA) and a generic unconjugated BA (uBA). The taurine-conjugates were not explicitly considered, as the BA pool in human serum consists of only ~15% taurine-conjugates, compared to ~45% glycine-conjugates and ~40% unconjugated BAs (Bathena et al., 2013). GCA and GDCA were selected, because their abundance in plasma showed the steepest decrease upon 7-day ODE-treatment in healthy individuals. GCDCA is the most abundant BA in human plasma and was therefore also included. The model developed may serve as a quantitative tool to evaluate various potential mode-of-actions in the framework of BA-associated diseases upon exposure to xenobiotics.

2 Material and Methods

2.1 Cell culture

Human colon carcinoma Caco-2 cells were purchased from the American Type Culture Collection (Rockville, MD, USA. The Caco-2 cells (passage number 15–28) were grown at 37 °C with 5% CO_2 in Modified Eagle's Medium (MEM) GlutaMax™ supplemented with 20% (v/v) fetal calf serum, 0.86% (v/v) 50 mg/mL L-glutamine-Penicillin-Streptomycin solution and 0.86% (v/v) 100 mM pyruvate as culture medium (CM), all purchased at Gibco BRL (Breda, The Netherlands). Cells were subcultured twice a week at 50-60% confluence using 0.05% trypsin-EDTA (Gibco BRL).

2.2 Cell viability assessment

Caco-2 cells were seeded at 40 000 cells/well in a 96-well plate and allowed to attach to the plate for 24 h. The effect of odevixibat (ODE) (99.85%, MedChemExpress, Monmoth Junction, NJ, USA) on the viability of Caco-2 cells 24h post-seeding was evaluated by using the WST-1 assay. Briefly, Caco-2 cells were exposed to 0–500 µM ODE for 24 h. ODE was dissolved in dimethyl sulfoxide (DMSO) (Merck KGaA, Darmstadt, Germany) and 200× diluted in CM. 0.5 µM potassium dichromate was used as a positive control. Subsequently, the cells were incubated with WST-1 reagent 2-(2-methoxy-4-nitrophenyl)-3-(4-nitrophenyl)-5-(2,4-disulfophenyl)-2H-tetrazolium (Sigma-Aldrich, St. Louis, MO, USA) at 37°C. For this, WST-1 was added

at 5% of the medium volume and the absorbance was measured at 440 nm and 620 nm with a SpectraMax iD3 multi-mode microplate reader (Molecular Devices; San Jose, CA, USA) after 60 min. Data were obtained by subtracting the 620 nm signal from the 440 nm signal. The cell viability was expressed as percentage of the solvent control group.

2.3 Intestinal Caco-2 monolayer barrier integrity assessment

Caco-2 cells were seeded at 180 000 cells/cm^2 in 24-well polycarbonate membrane inserts with 0.4 µm pore size (Corning Costar, Schnelldorf, Germany) and maintained in culture for 19-21 days. The integrity of Caco-2 cells was assessed using transepithelial electrical resistance (TEER) and/or the lucifer yellow assay. The TEER was measured with MilliCell® ERS-2 Epithelial Volt-Ohm Meter (Millipore, Amsterdam, The Netherlands). The TEER was measured prior to and post transport experiments, and data obtained from inserts with TEER values > 300 Ω × cm^2 were considered acceptable. For the lucifer yellow assay, the exposure medium was removed by rinsing the monolayers with Hank's balanced salt solution (Gibco BRL) supplemented with 10 mM HEPES (transport buffer), at pH 7.4. After that 50 µM lucifer yellow (Sigma-Aldrich) in DMSO (0.5% v/v) in transport buffer was added to the apical side of the culture insert. After 60 min, samples were taken basolaterally and the fluorescence was measured at 485/535 nm excitation/emission with a SpectraMax iD3 multi-mode microplate reader (Molecular Devices). Apparent permeability values (P_{app}) were calculated according to the following equation:

$$Papp = \frac{dQ}{dt} \times \frac{1}{A \times C0} \qquad \text{Eq. 1}$$

Where P_{app} is expressed in cm/s, dQ/dt is the change in the basolateral lucifer yellow concentration (nmol/s), A is the surface of the culture insert (cm^2) and C_0 is the initial apical lucifer yellow concentration (nmol/cm^3). Lucifer yellow P_{app} values <0.4 × 10^{-6} cm/s were considered acceptable (Wang et al., 2008).

2.4 Transport assays

For the transport assays, Caco-2 monolayers grown in culture inserts for 19-21 days were used. CM was removed and replaced with transport buffer. The cells were allowed to equilibrate for 30 mins. Next, transport buffer was removed, the test solution was added apically, and samples were taken at the basolateral side after 0-180 min of incubation. The test solutions contained 0.5% DMSO (v/v). In the first set of experiments, the cells were incubated with 5 µM glycocholic acid hydrate (GCA) (Sigma-Aldrich, ≥97%), deoxycholic acid (Sigma-Aldrich, ≥99%), glycochenodeoxycholic acid or glycodeoxycholic acid (Avanti, Birmingham, AL, USA, ≥99%) and samples were taken after 0, 30, 60, 90, 120, 150 and 180 min of incubation. These experiments were performed at 4°C and 37°C to distinguish between active and passive transport processes. After 180 minutes, samples were taken from the apical and basolateral chamber, and after washing twice with ice-cold PBS, the membrane was cut out of the culture insert and transferred to an Eppendorf tube containing 65% (v/v) MeOH in MilliQ. The samples were ultrasonicated for 15 mins (Bandelin Sonorex rk100), centrifuged for 15 mins at 15,000*g* and the supernatant was transferred to LC-MS/MS vials and stored at -20°C until analysis by LC-MS/MS. The amounts detected in the cells, apical and basolateral chamber were summed up to calculate the mass balance. Mass balances were considered acceptable when >80% of the initially added amount was recovered.

In further experiments, GCA was used as model BA. Due to the similar physicochemical properties of the tested BAs, it was assumed that the inhibitor constant (K_i) was independent of the substrate used. As described in section 2.8, literature was used to translate the experimentally obtained kinetic parameters for GCA to kinetic parameters for GCDCA and GDCA. Cells were incubated at 37°C with 5 µM GCA and an ODE concentration range (0.0005 – 5 nM) to determine the half inhibitory concentration (IC_{50}) of ODE on GCA transport. Next, the cells were incubated under time-optimized conditions with a concentration range of GCA to determine its kinetic parameters ($V_{max,app}$ and $K_{m,app}$). As sodium-binding drives the conformational changes in ASBT required for transport of its substrates (Al-Hilal et al., 2014), we performed transport assays in transport buffer without sodium to confirm the sodium-dependency of the transport and quantify the passive transport rate at different GCA concentrations. The active transport rate was determined by subtracting the passive transport rate from the total transport rate. The K_i was determined by incubating the cells with a concentration range of GCA in the presence of an ODE concentration close to the IC_{50}. Albeit it is unlikely that ODE affected passive sodium-independent transport, this was not experimentally confirmed in the current work. We assumed that the passive transport rate was not altered by addition of ODE. All transport assays were performed in triplicate.

2.5 Reusing culture inserts

To overcome the limited availability of culture inserts, they were reused up to one time based on the protocol by Kato et al. (2021). Briefly, the cells were removed from the culture inserts after performing a transport assay with 0.25% (v/v) trypsin-EDTA and kept sterile. Firstly, culture inserts were incubated with trypsin-EDTA for 1 h at 37°C. Trypsin-EDTA was aspirated and replaced with fresh trypsin-EDTA solution, both apical and basolateral. After 24 h, all trypsin-EDTA was removed and the culture inserts were washed twice with PBS, followed by two washes with sterile MilliQ water. Culture inserts were left to airdry and stored at 4°C until further use. We did not observe any significant differences in TEER values between new and recycled culture inserts. WST-1 showed similar cell viability (Fig. S1[1]), and we did not detect any BAs in the basolateral chamber when we performed a blank transport assay without BAs added. (Sharanek et al., 2015)

2.6 Bile acid profiling using LC-MS/MS

BA analysis was performed on a triple quadrupole LC-MS/MS system, model LCMS-8045 (Shimadzu Corporation, Japan) and based on our previous work (de Bruijn et al., 2022b; Wang et al., 2022; Zhang et al., 2022). GCA/GCDCA/GDCA/DCA were quantified. BAs in samples and standards were separated on a Kinetex C18 column (1.7 µm × 100 A × 50 mm × 2.1 mm, Phenomenex 00B-4475-AN, Utrecht, the Netherlands) using an ultra-high performance liquid chromatography (UHPLC)

[1] doi:10.14573/altex.2302011s1

system (Shimadzu) with gradient elution using MilliQ water (0.01% formic acid) and methanol/acetonitrile (50% v/v) as mobile phase A and B, respectively. In order to enhance chromatographic performance, a C18 2.1 mm security guard (Phenomenex AJ0-8782) precolumn was used.

Samples were injected (2 µL) onto the column equilibrated in 30% B at a flow rate of 0.4 mL/min. Initially, the mobile phase composition was 30% B, followed by a linear ramp to 70% B until 10.0 min. A linear change to 98% B was executed until 11.0 min, which was held for another 7 min before returning to 30% B at 19.0 min and remained until 25 min. The column temperature was set at 40°C and the sample tray temperature was set at 4°C.

The mass spectrometer (MS) used electrospray ionization (ESI) in negative ion mode. The ESI parameters were as follows: Nebulizing gas flow, 3L/minutes; drying gas flow and heating gas flow, 10 L/minute; Interface temperature, 300°C; desolvation temperature, 526°C; heat block temperature, 400°C. Selective ion monitoring (SIM) and multiple reaction monitoring (MRM) were used for the detection of the bile acids.

Limit of Detection (LOD) and Limit of Quantification (LOQ) of BA concentration in transport buffer were based on the signal-to-noise ratio. Signal-to-noise ratios of 3:1 and 10:1 were used as these are generally accepted for estimating LOD and LOQ, respectively (Shrivastava and Gupta, 2011). Here, LOD and LOQ were set to BA concentrations in transport buffer that resulted in a signal-to-noise ratio of at least 3:1 or 10:1, respectively. For subsequent calculations concentrations <LOD were set to 0 and concentrations ≥LOD and <LOQ were set to 0.5 × LOQ. As we observed a matrix effect on the sensitivity of our analytical method, standards for the calibration curve were prepared in transport buffer. Data were collected and processed using the LabSolutions software (Shimadzu). The MS parameters, LODs and LOQs are provided in Table S1[1].

2.7 Data analysis

R version 4.1.0. was used for all data analysis and simulations[2]. The R package tidyverse version 1.3.1[3] was used for data exploration and visualization. Statistical significance was determined by a one-way ANOVA followed by Bonferroni's correction for multiple tests. Results were considered statistically significant when $p<0.05$. The appropriate model to estimate the IC_{50} of ODE-mediated inhibition of GCA transport was selected by minimizing the logLikelihood. The best fit was achieved by the three-parameter log-logistic function using the package 'drc' version 3.0.1 (Ritz et al., 2015). The lower and upper limit were constrained to 0 and 100 (%), respectively, and the Hill slope was variable. From the Lineweaver-Burk plot (Lineweaver and Burk, 1934), we derived that ODE inhibited GCA transport in a competitive nature. Previous research showed that *in vitro* permeability is affected by unstirred water layers in the vicinity of the culture insert and the culture insert itself, which is jointly referred to as the aqueous boundary layer (ABL). The ABL acts as a permeability barrier in transport experiments and was previously shown to bias kinetic estimates (Balakrishnan et al., 2007). Therefore, taking into account the aqueous boundary layer (ABL) resistance, the transport rate could be described as (Balakrishnan et al., 2007) (Eq. 2):

$$V_{app} = \frac{P_{ABL} \times \frac{V_{max,app}}{K_{m,app}\left(1+\frac{[\mathrm{ODE}]\times F_{ub}}{K_i}\right)+[GCA]\times F_{ub}}}{P_{ABL}+\frac{V_{max,app}}{K_{m,app}\left(1+\frac{[\mathrm{ODE}]\times F_{ub}}{K_i}\right)+[GCA]\times F_{ub}}} \times [\mathrm{GCA}] \times F_{ub} \qquad \text{Eq. 2}$$

Where V_{app} is the active apparent GCA transport rate from the apical to basolateral chamber in nmol min^{-1} cm^{-2}, P_{ABL} the permeability across the ABL in cm/min, $V_{max,app}$ the maximal apparent active GCA transport rate nmol min^{-1} cm^{-2}, [GCA] the concentration of GCA in nmol cm^{-3}, F_{ub} the fraction unbound *in vitro*, $K_{m,app}$ the apparent Michaelis-Menten constant in nmol cm^{-3}, [ODE] the concentration of ODE in nmol/L and K_i the inhibitor constant in nmol/L. P_{ABL} was set to 4.2×10^{-3} cm min^{-1} (Balakrishnan et al., 2007). Fraction unbound *in vitro* was set to 1, i.e., the nominal concentration equaled the free concentration. This was justified as the transport buffer did not contain any protein (Gilbert-Sandoval et al., 2020). The parameters were optimized using the 'nls' function in R (R Core Team, 2022).

2.8 Physiologically based kinetic (PBK) model

To describe the synthesis, absorption, distribution, metabolism, and excretion of BAs, four physiologically based kinetic (PBK) submodels were constructed; a glyochenodeoxycholic acid (GCDCA), a glycocholic acid (GCA), a glycodeoxycholic acid (GDCA) and an unconjugated BA (uBA) model. Combined these BAs represent ~85% of the BA pool in human serum (Bathena et al., 2013). The PBK submodels were based on our previous work (de Bruijn et al., 2022a). Modifications were made to expand the model to four BAs instead of one lumped BA pool, to describe intestinal transit and absorption in more detail and the liver as a permeability-limited model.

Briefly, each submodel consisted of separate compartments representing gall bladder, intestine, blood, rapidly perfused tissue, slowly perfused tissue, adipose tissue and extra- and intracellular water in liver. Figure 1 displays the conceptual model. In PBK models, organs are typically described using perfusion-limited models. This modeling approach assumes that compounds diffuse passively into the organ's water and are instantly homogenously distributed throughout the organ (Rietjens et al., 2011). For transporter-mediated uptake, however, permeability and not perfusion is the rate-limiting step. Therefore, perfusion-limited

[2] https://www.r-project.org/
[3] https://cran.r-project.org/web/packages/tidyverse/index.html

Fig. 1: Conceptual model

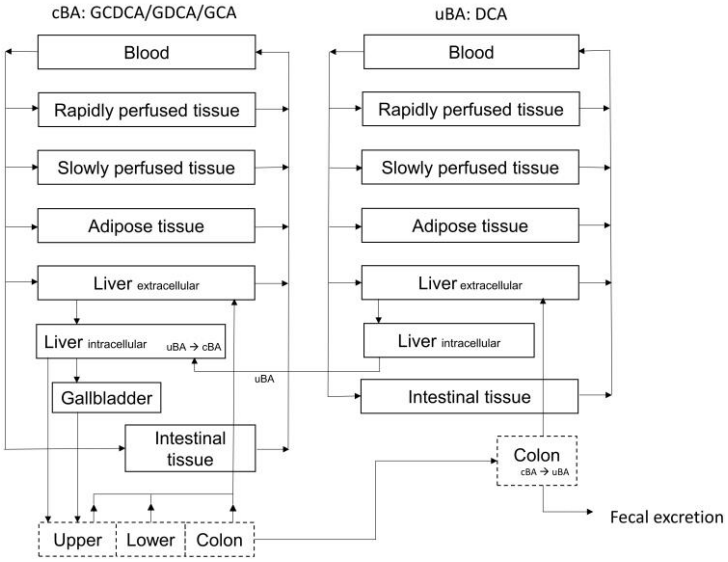

cBA=conjugated BA, uBA=unconjugated BA, GCA=glycocholic acid, GCDCA=glycochenodeoxycholic acid, GDCA=glycodeoxcycholic acid, DCA=deoxycholic acid

Tab. 1: Physicochemical properties of the model BAs used to calculated the blood:tissue partition coefficients

	GCDCA	GCA	GDCA	DCA	Ref.
pKa	3.77	3.77	4.6	4.65	(Law et al., 2014), (Schwarz et al., 1996)
logP	2.12	1.65	2.25	3.5	(Roda et al., 1990)
MW	449.62	465.6	449.62	392.57	
Fraction unbound	0.061	0.088	0.055	0.02	Calculated, (Lobell and Sivarajah, 2003)

models cannot be used and a permeability-limited model should be used to simulate transporter-mediated uptake (Jamei et al., 2014). In these models, the respective organ is divided in an extracellular water and intracellular water compartment. In the present BA model, the liver compartment was modelled in this way to enable description of the NTCP-mediated active transport from the extracellular to the intracellular liver water compartment and of the BSEP-mediated active transport from the intracellular water compartment to the bile. The extracellular water compartment is in instantaneous equilibrium with the blood in the vascular space and serves as a barrier compartment for entry into the intracellular tissue compartment. As sinusoidal efflux is low under normal physiological conditions (Dawson et al., 2009), this process was not included to limit model complexity. The extracellular water:plasma partition coefficients were calculated by a quantitative property-property relationship (Peyret et al., 2010). The BA fraction available for transport and metabolism in intracellular and extracellular water was set to 1, since transcellular trafficking of BAs is highly efficient and effectively mediated by bile acid-binding proteins (BABPs) (Toke, 2022). Tissue:plasma partition coefficients for the BAs were calculated by a method described in literature (Rodgers and Rowland, 2006) and obtained via the QIVIVE toolbox (Punt et al., 2020). Recent work showed that the method of Lobell and Sivarajah (2003) to describe the fraction unbound resulted in the most accurate model predictions (Punt et al., 2022), hence this method was used here. As deoxycholic acid (DCA) is the most abundant uBA in human serum, DCA's physicochemical properties were selected to describe uBAs. The physicochemical properties of the BAs used to calculate the tissue:plasma partition coefficients are described in Table 1.

The enterohepatic circulation was included by a circulation of BA between the liver, gall bladder and intestine. BAs were *de novo* synthesized in the liver and excreted via the intestinal compartments into the feces. Hepatic BA efflux was simulated to be actively transported from the liver directly into the intestine or to the gallbladder by BSEP following Michaelis-Menten kinetics. The BSEP-mediated effluxes of BAs were described by the following equation (Eq. 3):

$$V_{BSEP} = \frac{V_{max,BSEP} * [CVL]}{K_{m,BSEP} + [CVL]} \qquad \text{Eq.3}$$

Where V_{BSEP} is the BSEP-mediated efflux of BAs from the liver in µmole/h, $V_{max,BSEP}$ is the maximum rate of BSEP-mediated BA efflux from the liver µmole/entire liver/hour, [CVL] the free concentration of BAs in the liver in µmole/L and $K_{m,BSEP}$ the Michaelis-Menten constant in µmole/L for BSEP-mediated BA efflux.

The $V_{max,app}$ and $K_{m,app}$ for BSEP-mediated transport of GCDCA and GCA were taken from literature as obtained in a vesicular transport assay in a baculovirus-infected Sf9 system (Kis et al., 2009) and scaled to the *in vivo* situation as described previously (de Bruijn et al., 2022a). The authors showed that the $V_{max,app}$ values in the vesicular transport assay increased upon the addition of physiological levels of cholesterol, hence, these values were used in the current PBK model. The literature study investigated GCA and GCDCA, but not GDCA (Kis et al., 2009). Therefore, the kinetic data for BSEP-mediated GDCA transport were extracted from a study with transfected HEK293 cells reported by Notenboom et al. (2018). The $V_{max,app}$ of BSEP-mediated transport as obtained by Notenboom et al. (2018) was initially measured in pmol/min/mg protein. To make the measurements consistent with GCA and GCDCA, the $V_{max,app}$ values for GDCA were converted to µmole/min/mg BSEP using GCDCA mediated transport, which was measured in both the study by Notenboom et al. (2018) and Kis et al. (2009), as a reference. Consequently, the GDCA simulations were performed with $V_{max,app,GDCA} = V_{max,app,GCDCA[Sf9\ vesicles]} / V_{max,app,GCDCA[HEK293\ vesicles]} \times V_{max,app,GDCA[HEK293\ vesicles]} = 8.4$ µmole/min/mg BSEP.

The intestine was divided in three compartments: 1) the upper intestines (duodenum + jejunum), where BAs are passively absorbed, 2) the lower intestine (ileum), where BAs are absorbed through a carrier-mediated process, and 3) the colon, where BAs are rapidly deconjugated and subsequently passively absorbed. Transit times were taken from the modified GI transit absorption (GITA) model introduced by Kimura and Higaki (2002), different transit times were used during fasting (17:30 – 8:00) and fed state. During daytime, three meals and gall bladder contractions were simulated, i.e., at 8:00, 12:00 and 16:00. The parameters describing passive uptake were derived from perfusion studies (Krag and Phillips, 1974), and were assumed to be the same for jejunum and colon.

Kinetic parameters for active GCA transport were derived from our Caco-2 study. For scaling to the *in vivo* situation, the experimentally derived $V_{max,app}$ was multiplied by the total surface of the ileum and an empirical scalar, which was calculated as follows (Eq. 4):

$$SF = \pi d \times l \times ES \qquad \text{Eq. 4}$$

Where S is the ileal surface in cm^2, d is the diameter of the ileum (cm), l is the length of the ileum (cm) and p represent the mathematical constant of 3.14. A diameter and length of 5 and 300 cm were taken, respectively (Kararli, 1995). ES is an empirical scalar to better approximate the *in vivo* situation and was set to 2.8. ES accounts for inherent differences between Caco-2 cells and the human entire ileum, such as variations in ASBT expression or activity, tissue complexity and cellular interactions.

Subsequently, the calculated GCA $V_{max,\ in\ vivo}$ was used to scale the relative $V_{max,\ invitro}$ of GCDCA and GDCA obtained from literature to the *in vivo* situation. These values were retrieved from an ASBT-Madin-Darby canine kidney (MDCK) monolayer assay (Balakrishnan et al., 2006). The authors reported a large variation in ASBT expression levels between studies, therefore, they measured taurocholic acid flux to serve as a normalizing approach. In this way they obtained a V_{max} relative to the TCA V_{max} for 15 different BAs. We used the following equation to scale the relative V_{max} ($V_{max,BA,rel}$) to the *in vivo* V_{max} ($V_{max,BA,\ in\ vivo}$):

$$V_{max,BA,in\ vivo} = V_{max,BA,rel} \times \frac{V_{max,GCA,in\ vivo}}{V_{max,GCA,rel}} \qquad \text{Eq. 5}$$

Where $V_{max,BA,\ in\ vivo}$ is the *in vivo* maximal ASBT-mediated transport rate for the BA of interest, $V_{max,BA,rel}$ the maximal ASBT-mediated transport rate for the BA of interest relative to TCA, $V_{max,GCA,invivo}$ the maximal ASBT-mediated GCA transport rate obtained from our *in vitro* studies and scaled to the *in vivo* situation (Eq. 4) and $V_{max,GCA,rel}$ the maximal ASBT-mediated transport rate of GCA relative to TCA. For GDCA and GCDCA $K_{m,app}$ values from Balakrishnan et al. (2006) were incorporated in the PBK model without any further scaling. For GCA, we averaged our experimentally derived $K_{m,app}$ and the $K_{m,app}$ values from Balakrishnan et al. (2006). The effects of the different values for $K_{m,app}$ on the outcomes of the model calculations were also analyzed.

BAs escaping ileal absorption enter the colon, where they are rapidly and instantly deconjugated by the gut microbiome (Zhang et al., 2022). Upon reabsorption and entering the liver, these uBAs are rapidly and instantly conjugated (Falany et al., 1994). This is supported by the fact that only 0.3% of hepatic BAs exist in its unconjugated form (Garcia-Canaveras et al., 2012). Consequently, the intestinal deconjugation and hepatic conjugation rates were set to 1000 hr^{-1}.

Hepatic uptake of conjugated BAs from the extracellular water into the intracellular water was simulated as a permeability limited NTCP-mediated process. uBAs are taken up via passive diffusion (Notenboom et al., 2018). In this study, it was assumed that the diffusion of uBAs from the extracellular water to the intracellular water occurs at a rate equivalent to the hepatic blood flow. The $K_{m,app,}$ $V_{max,app}$ and scaling factor for *vitro-in vivo* scaling for the NTCP-mediated transport were obtained from a study with NTCP-transfected HEK293 cells (Notenboom et al., 2018). These authors determined the scaling factor by comparing the NTCP abundance in NTCP-transfected HEK293 cells and human liver tissue. The hepatic BA uptake rate was described by the following equation (Eq. 6):

$$\frac{d}{dt} AL_{IW,upt} = \frac{V_{max,NTCP} * [CVL_{EW}]}{K_{m,\mathrm{NTCP}} + [\mathrm{CVL}_{EW}]} \qquad \text{Eq.6}$$

Where d/dt $AL_{iw,upt}$ is the BA uptake rate into the intracellular water in µmole/entire liver/hour, CVL_{EW} the effluent concentration of the extracellular water, $V_{max,NTCP}$ is the maximal NTCP-mediated uptake rate in µmole/entire liver/hour, and $K_{m,NTCP}$ the Michaelis-Menten constant in µmole/L for NTCP-mediated uptake. The $V_{max,NTCP}$ in pmol min^{-1} 10^{-6} hepatocytes was extrapolated to units appropriate for the PBK model, *i.e.* µmoles $hour^{-1}$ entire $liver^{-1}$, by multiplying the $V_{max,NTCP,}$ with the hepatocellularity (10^6 hepatocytes/g liver) (Barter et al., 2007), weight of the liver (g) (Soars et al., 2002), 60 to convert minutes to hours and 10^{-6} to convert pmol to µmol. OATP-transporters were not explicitly considered, because rat Ntcp was proven to be responsible for more than 80% of conjugated bile acids (TCA) uptake (Kouzuki et al., 1998) and we assumed a comparable ratio in human hepatocytes. Instead, $V_{max,NTCP}$ was divided by 0.8 to account for the additional effects of OATP-mediated transport. As an up to 18-fold difference in GCDCA affinity for NTCP was reported in literature (Notenboom et al., 2018; Jani et al., 2018), GCDCA simulations were ran with the K_m as reported by Notenboom et al., a 18-fold reduced K_m and the average of these two values.

Lastly, given that the inhibition of ASBT by ODE was shown to be competitive in nature, the effects of ODE on the plasma BA concentrations was simulated by adjusting the K_m of ASBT-mediated uptake with a modulation factor of $1 + \frac{[\mathrm{ODE}] \times F_{ub}}{Ki}$ as described in Eq. 2. Where ODE is the total concentration of ODE in the ileum, F_{ub} is the fraction unbound in the ileum *in vivo* and K_i the inhibitory constant as derived from our experiments. As ODE is poorly absorbed, no absorption was simulated and the full dose was assumed to be equally distributed over 9 L of gastrointestinal fluid (Deeks, 2021; Hendriksen et al., 2003). F_{ub} in the ileum was set equal to the F_{ub} in plasma, *i.e.* 0.3% (EMA, 2021).

The differential model equations were encoded and solved using the package 'RxODE' version 1.1.5[4]. The model code and input parameters are available in the supplementary files in .docx[1] and .xlsx[5] format, respectively.

[4] https://nlmixrdevelopment.github.io/RxODE/
[5] doi:10.14573/altex.2302011s2

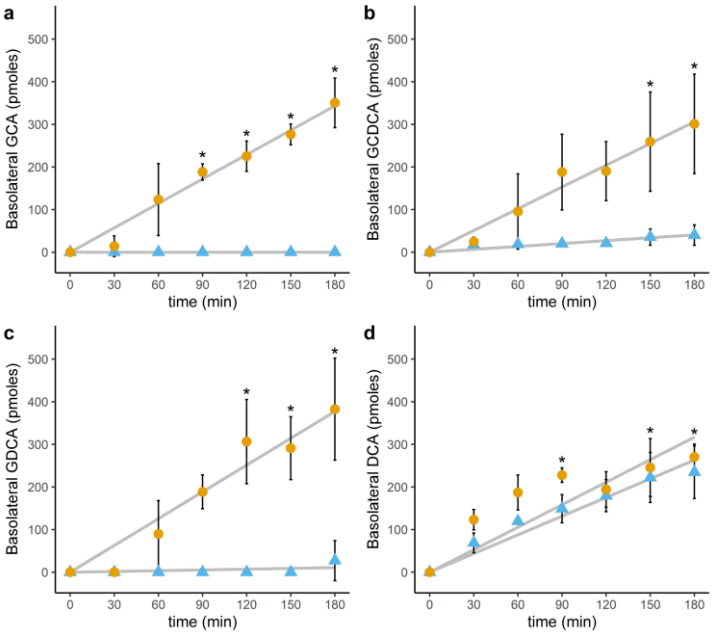

Fig. 2: Bile acid transport across a Caco-2 monolayer measured during 180 min at 37°C (orange circles) or 4°C (blue triangles)
500 pmoles of GCA/GCDCA/GDCA/DCA were added to the apical chamber at t=0, and samples were taken from the basolateral chamber at different timepoints. Data are expressed as mean ± SD, N=3. LOD/LOQ are reported in Table S1[1]. GCA=glycocholic acid, GCDCA=glycochenodeoxycholic acid, GDCA=glycodeoxcycholic acid, DCA=deoxycholic acid. Significance compared to t=0 min was assessed with a one-way ANOVA followed by post hoc tests using Bonferroni's correction. Statistically significant differences in basolateral amount of bile acids compared to t=0 are indicated with *.

2.9 Sensitivity analysis

To assess the influence of the parameters on the model outcome, a local sensitivity analysis was performed for the C_{max} of BAs using the package 'FME' version 1.3.6.2 (Soetaert and Petzoldt, 2010). The sensitivity analysis for T_{max} was performed manually. Based on the method reported by Evans and Andersen (2000), the sensitivity coefficients (SCs) for the model parameters were calculated as follows:

$$SC = \frac{C' - C}{P' - P} \times P/C \qquad \text{Eq. 7}$$

where C indicates the initial value of the model output, C′ indicates the modified value of the model output resulting from an increase in the parameter value. P indicates the initial parameter value and P′ indicates the modified parameter value after a 5% increase of its value, keeping all other parameters at their original value.

3 Results

3.1 Bile acids cross Caco-2 monolayers via passive and active transport

19-21-day old Caco-2 monolayers grown in culture inserts were apically exposed to 500 pmol of four BAs to optimize the incubation time for obtaining kinetic parameters and study the mode of transport. We observed apical-to-basolateral transport of glyochenodeoxycholic acid (GCDCA), glycocholic acid (GCA), glycodeoxycholic acid (GDCA) and deoxycholic acid (DCA). Transport of GCA was observed exclusively at 37°C (>300 pmol), no transport was detected at 4°C. Comparable amounts GCDCA and GDCA were transported at 37°C, while for these two conjugated BAs limited transport at 4°C was observed especially at 180 min, albeit so low that it could not be quantified (<LOQ) (Fig. 2). DCA transport was observed at both 4°C and 37°C without a significant effect of temperature on the total amount transported after 180 mins. For all four BAs a linear relationship between time and the amount of BAs transported was observed at 37°C (Pearson's correlation coefficient 0.79-0.94, p<0.05).

3.2 ODE inhibits GCA transport dose-dependently

To assess the effect of the known ASBT-inhibitor ODE on the GCA apical-to-basolateral transport over Caco-2 cells, 500 pmol of GCA and a concentration range of ODE were added to the apical chamber of a culture insert with a confluent monolayer of Caco-2 cells and the basolateral GCA was measured. The results from the WST-1 assay confirmed that ODE concentrations up to 500 µM did not affect cell viability (Fig. S2A[1]). Combined exposure to the increasing concentrations of ODE and 500 pmol GCA did not have statistically significant effects on TEER values (Fig. S2B[1]). We observed that ODE inhibited GCA apical-to-basolateral transport in a dose-dependent manner (Fig. 3), and the IC_{50} value was estimated to be 0.04 nM ODE.

3.3 ODE inhibits GCA transport in a competitive manner

Finally, the Caco-2 transport assay was used to obtain kinetic parameters for the PBK model. Our results showed that the GCA transport rate saturated with increasing GCA concentrations. A relatively small amount of GCA (<16% of the total GCA

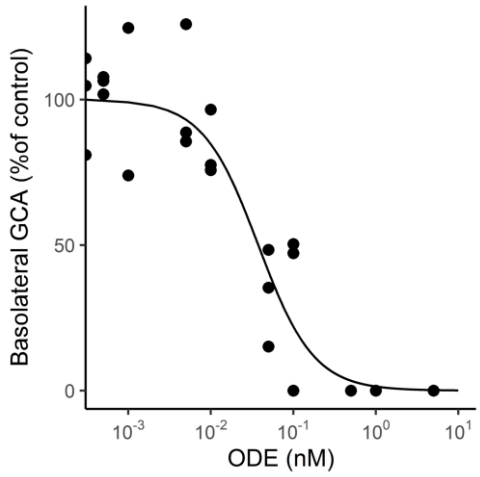

Fig. 3: Odevixibat (ODE)-dependent inhibition of glycocholic acid (GCA) transport across Caco-2 monolayers
Values are normalized to the control. N=3.

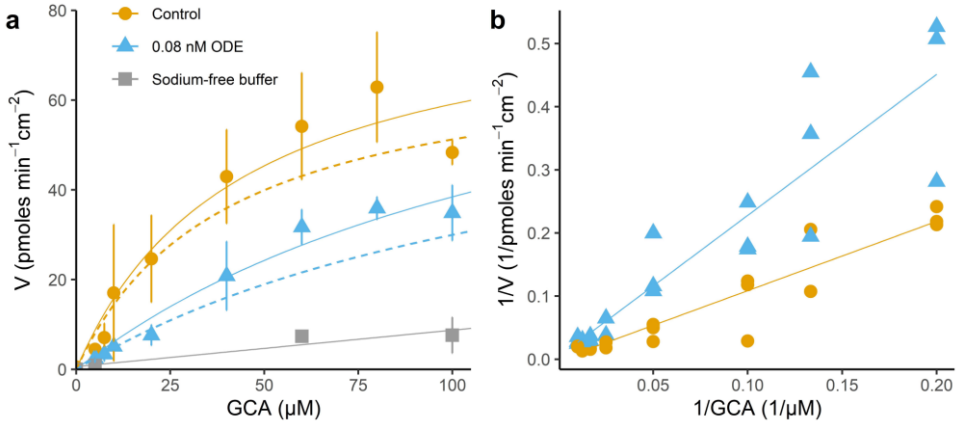

Fig. 4: Concentration-dependent transport of glycocholic acid (GCA) across Caco-2 monolayers and inhibition by odevixibat (ODE)
a) GCA transport rate after incubation with control buffer in the presence or absence of 0.08 nM ODE or with sodium-free buffer. The solid lines indicate the total transport; the dashed lines indicate active transport only, and were calculated by subtracting the transport rate in absence of sodium from the total transport rate. Values represent the mean ± SD, N=3. b) Lineweaver-Burk plot. Lines with and without ODE share the same intercept, but not slope (ANOVA).

transport) was transported in the absence of sodium, i.e., via passive processes. The active transport rate was determined by subtracting the passive transport rate from the total transport rate (Fig. 4a). The nature of ODE inhibition of GCA transport was evaluated using a Lineweaver-Burk plot (Fig. 4b). For this the reciprocal of the GCA concentration (1/GCA) was plotted versus the reciprocal of the reaction speed (1/V), either with or without 0.08nM ODE. ANOVA demonstrated that the slope, but not the intercept, was significantly different between the two curves. Hence, incubation with ODE increased the $K_{m,app,}$ but did not affect $V_{max,app}$, indicating that ODE inhibits GCA transport in a competitive manner. Consequently, the following parameters were obtained for active GCA transport from Eq. 2: $V_{max,app}$=71.5 pmol min^{-1} cm^{-2}, $K_{m,app}$=22.5 µM, K_i=0.02 nM.

3.4 Postprandial bile acid kinetics are readily described by the PBK model

The parameters for active GCA transport obtained using the Caco-2 transport assay were incorporated in the PBK model using the total ileal surface and an empirical scalar for *in vitro-in vivo* scaling, as described in Eq. 4. The PBK model describes the synthesis, absorption, distribution, metabolism, and excretion of BAs for a healthy individual. For the first set of predictions, meals were simulated at 8:00, 12:00 and 16:00. This meal regimen was in accordance with the regimen used in the study of Hepner and Demers (1977) of which the data were used to validate our predictions. A second *in vivo* dataset available for model evaluation describes the postprandial BA kinetics for 8 hours after one meal (Lamaziere et al., 2020). The observed and predicted plasma BA-time profiles are displayed in Figure 5. GCA and uBA postprandial kinetics were predicted within 2-fold of both *in vivo* data sets, GDCA was predicted within 2-fold of the data obtained by Hepner and Demers (1977), but the model overpredicted the other *in vivo* data set with 25-fold (Lamaziere et al, 2020), which also underlines the interstudy and/or interindividual differences. Three scenarios with different K_m values for NTCP-mediated GCDCA transport were simulated (Fig. 6). K_m values of 10, 0.6 and 5.3 µM, derived from Notenboom et al. (2018), Jani et al. (2018) and the average of these two studies, respectively, were used to run the simulations. The GCDCA C_{max} decreased with a decreasing K_m. The lowest K_m value resulted in only a minor increase in plasma GCDCA levels compared to the fasting state. The best fit to the *in vivo* data was obtained when the K_m values of the two studies were averaged. For further simulations, the averaged K_m value reported

ALTEX, accepted manuscript
published July 27, 2023
doi:10.14573/altex.2302011

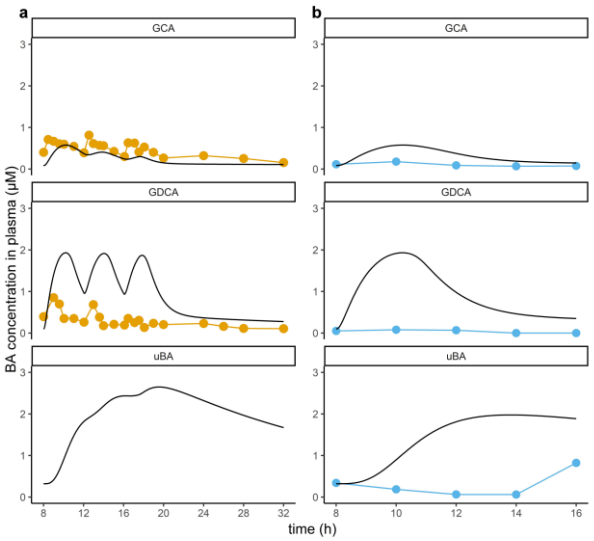

Fig. 5: Observed and predicted postprandial bile acid kinetics
Black solid line=prediction**.** a) Meals were simulated at 8:00, 12:00 and 16:00. Orange circles=in vivo data obtained from Hepner and Demers (1977). b) A single meal was simulated at 8:00. Blue circles= in vivo data obtained from Lamaziere (2020). GCA=glycocholic acid, GDCA=glycodeoxycholic acid; uBA=unconjugated bile acids

Fig. 6: Observed and predicted postprandial GCDCA kinetics using different kinetic parameters for NTCP affinity

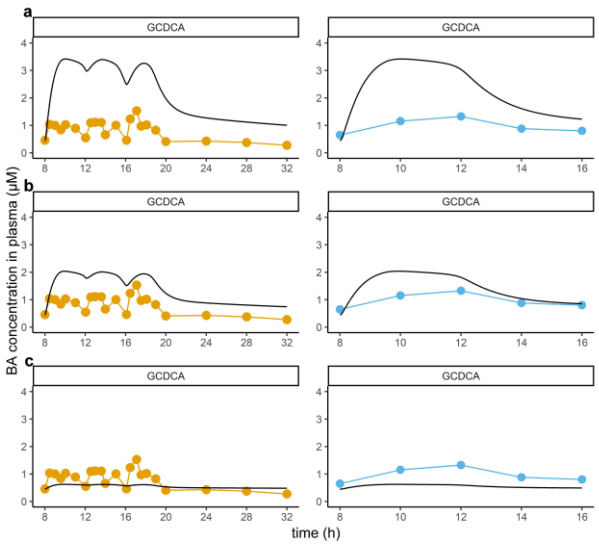

Black solid line=prediction**.** Left column: Meals were simulated at 8:00, 12:00 and 16:00. Orange circles=in vivo data obtained from Hepner and Demers (1977). Right column: Meal was simulated at 8:00. Blue circles= in vivo data obtained from Lamaziere (2020). a) K_m=10 µM (Notenboom et al. (2018), b) K_m=5.3 µM (average Notenboom et al. (2018) and Jani et al. (2018) c) K_m=0.568 µM (Jani et al. (2018)). GCDCA=glycochenodeoxycholic acid

was used for GCDCA, given its better fit to the *in vivo* data. We used the average of our experimentally derived ABL-corrected $K_{m,app}$ and the $K_{m,app}$ reported in literature for ASBT-mediated GCA transport. The influence of different K_m values on the postprandial GCA kinetics are depicted in Figure S3[1].

3.5 ODE lowers the simulated plasma levels of conjugated bile acids

The effects of ODE-administration on the plasma and colonic BA levels were simulated using the perfusion-limited liver model and the two different sets of kinetic parameters to describe BSEP-mediated hepatic GDCA efflux. The simulated change in total plasma BAs was within the 95% confidence interval (CI) observed in a previous phase I clinical trial (Graffner et al., 2016). The current PBK model only simulated the concentrations of GCA, GCDCA, GDCA and uBA, while tauro-conjugates also circulate through the human body. Tauro-conjugates represent ~15% of the BAs in human plasma and to correct for the presence of tauro-conjugates, the predicted BA concentrations in Figure 7a-c were divided by 0.85 (black dashed line) to present a better estimate of the whole BA pool. The plasma levels of conjugated BAs (GCA, GCDCA and GDCA) were predicted by the PBK model to decrease ODE dose-dependently, while the uBA plasma levels showed a slight increase (Fig. 7b). The uBA levels in the colon were predicted to increase with increasing ODE dosages (Fig. 7c).

3.6 Sensitivity analysis

To assess the influence of the parameters on the C_{max} and T_{max}, a local sensitivity analysis was performed. Figure 8A shows that parameters related to the active transport of GCA over the intestine and from extracellular to intracellular water and their scaling have a strong influence on the GCA C_{max} (absolute normalized sensitivity coefficient >0.5). Not only the maximal ASBT-mediated intestinal uptake rate (VmaxASBTc_GCA), but also the kinetic parameters describing NTCP-mediated hepatic uptake (VmaxNTCPc_GCA and KmNTCP_GCA) strongly influence the model outcome. ES_all and surface_all are used for the scaling of VmaxASBTc_GCA, and Hep_all_GCA is included in the scaling of VmaxNTCP_GCA, but also in the BSEP-mediated hepatic efflux. Furthermore, the ileal transit time in the fed stad (kti_fed), blood:plasma (BP_all) ratio, body weight (BW_all) and the factor used incorporate OATP-mediated transport negatively (SF_OATP) negatively impact GCA C_{max}. The portal blood flow (QPVc_all) has a positive influence on the GCA C_{max}. The sensitivity analyses for GCA, GCDCA

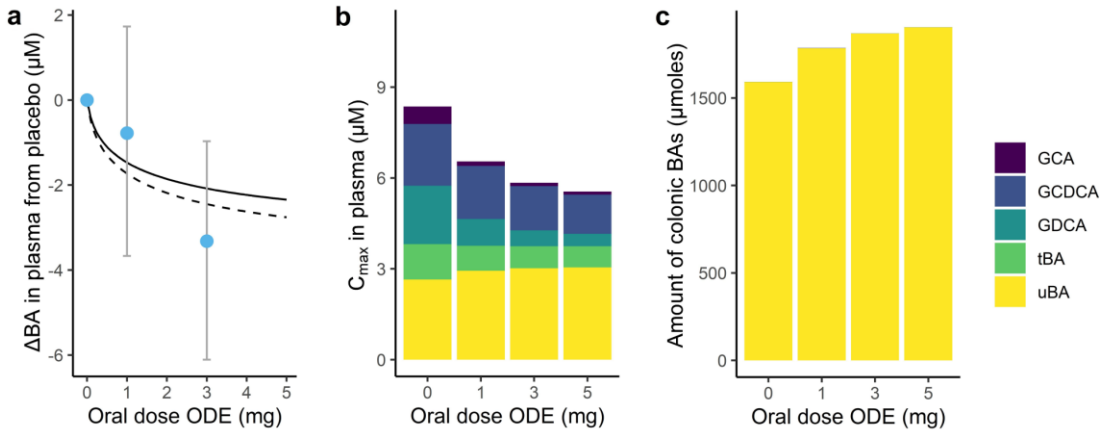

Fig. 7: Bile acid levels in individuals receiving the placebo or ODE
a) Predicted versus observed change in maximal total plasma bile acids compared to the placebo on day 1 of ODE treatment. Blue circles are in vivo data retrieved from Graffner (2016)(mean± 95% CI), black solid line is the prediction for the sum of GCA, GCDCA, GDCA and uBA, black dashed line is the prediction corrected for tauroconjugates b) Predicted BA C_{max} for different BAs and c) Predicted maximal amounts of colonic BAs; note that in colon the amounts of the conjugated BAs (GCA, GCDCA and GDCA) were <0.6 μmoles. GCA=glycocholic acid, GCDCA=glycochenodeoxycholic acid; GDCA=glycodeoxycholic acid; tBA=tauroconjugated bile acids; uBA=unconjugated bile acids

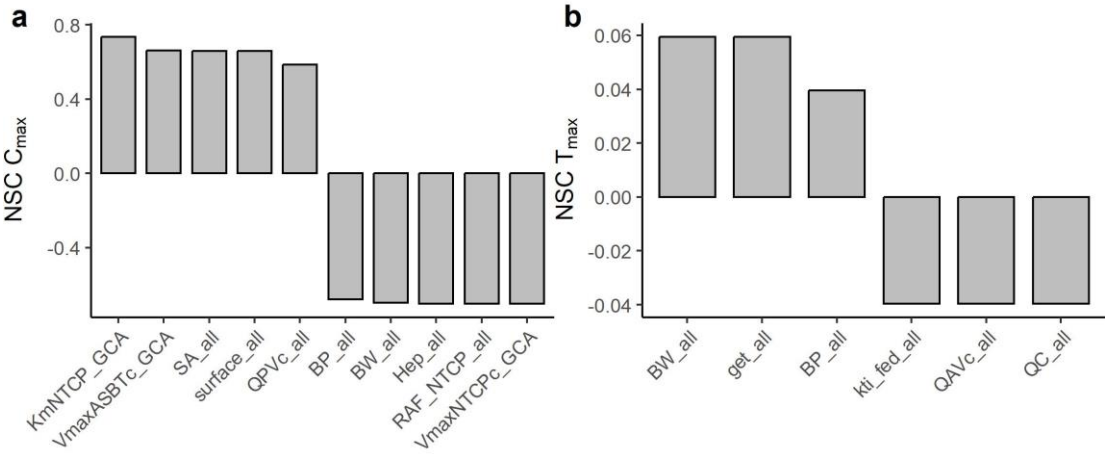

Fig. 8: Sensitivity analysis of the influence of the PBK model parameters on the predicted outcomes
a) Sensitivity analysis for maximal systemic GCA concentration in plasma (C_{max}). Only parameters with an absolute normalized sensitivity coefficient (NSC) > 0.5 are shown. b) Sensitivity analysis for the time taken before reaching C_{max} (T_{max}). Only parameters with an absolute normalized sensitivity coefficient (NSC) > 0.03 are shown. KmNTCP=Michaelis–Menten constant for NTCP-mediated BA uptake in the liver, VmaxASBTc= maximal ASBT-mediated GCA absorption rate over the ileal epithelium, ES=empirical scalar for in vitro-in vivo extrapolation of Caco-2 derived kinetic parameters, surface=cylindrical surface of ileum, QPVc=fraction of blood flow through the portal vein, BP=blood:plasma ratio, Hep=hepatocellularity, SF_OATP=scaling factor to adjust hepatic uptake for OATP-mediated uptake, VmaxNTCPc= maximal NTCP-mediated GCA hepatic uptake rate, BW=body weight, get=gall bladder ejection time, kti_fed=ileal transit time in fed state, QAVc=fraction of blood flow to liver through the arterial vein. QC=cardiac output. _GCA indicates a parameter specifically for the GCA submodel, _all indicates a parameter that is shared for all BA submodels.

and GDCA are roughly similar (Fig. S4[1]), while uBA C_{max} is not strongly influenced by transporter-mediated processes or their scaling factors. Even though parameters related to BSEP-mediated active hepatic efflux do not have a strong influence on plasma BA C_{max}, they were shown to strongly influence the maximal intracellular concentrations of GCA, GCDCA and GDCA in the liver (Fig. S5[1]). Figure 8B shows that the gall bladder emptying time (get_all) and body weight (BW) have the strongest delaying influence on the GCA T_{max}, while the cardiac output (QC_all), the fraction of the arterial blood flow to the liver (QAVc_all) and ileal transit time in fed state (kti_fed) have the strongest accelerating influence on GCA T_{max}. The sensitivity analyses for the other BAs consistently identified intestinal transit time as an important parameter for T_{max} (Fig. S6[1]). It should be noted that the normalized sensitivity coefficients for T_{max} are around one order of magnitude smaller than those for C_{max}.

4 Discussion

For this work the aim was to predict the effects of ASBT-inhibition on systemic plasma levels and by that obtain mechanistic insights in whole-body BA homeostasis, with a focus on the gut-liver axis. To this end, we obtained kinetic parameters for the active intestinal glycocholic acid (GCA) transport across Caco-2 monolayers and incorporated these in a physiologically based kinetic (PBK) model describing the synthesis, absorption, distribution, metabolism and excretion of BAs. The current study

shows that Caco-2 cells transported GCA in an active and sodium-dependent manner, indicating that apical sodium-dependent bile acid transporter (ASBT) functionality is maintained in Caco-2 cells. Subsequently, Caco-2 cells were applied to obtain kinetic parameters for ASBT-mediated GCA transport over the intestinal epithelium. These parameters were incorporated in the PBK model after *in vitro* to *in vivo* scaling. The integration of active intestinal uptake in the PBK model allowed us to incorporate dose-dependent BA transport inhibition induced by the selective and reversible ASBT inhibitor odevixibat (ODE). Our PBK model predicted that the plasma concentrations of conjugated BAs decrease upon ODE treatment, while unconjugated BA plasma concentrations are predicted to slightly increase. These predictions were in line with observations in the only available clinical phase I study reporting systemic plasma and fecal bile acids (Graffner et al., 2016). The sensitivity analysis revealed that active transport processes strongly influence the maximal conjugated BA concentration in plasma (C_{max}). The affinity of conjugated BAs for Na^+-taurocholate co-transporting polypeptide (NTCP) as well as the maximal rate of ASBT-mediated ileal uptake (Vmax_ASBTc) and the parameters required for its scaling have a strong positive influence on the C_{max}. Our results indicate that accurate estimates for active ileal and hepatic transport processes are key for high predictive power of a PBK model describing BA homeostasis. The developed BA PBK model is to our knowledge the first PBK model that includes experimentally derived data for NTCP-mediated hepatic BA uptake, BSEP-mediated hepatic BA efflux and ASBT-mediated ileal BA uptake.

In the current study it was shown that Caco-2 cells transport BAs via active transport and passive diffusion processes. Although no differences were observed in the total transport of GCA, glyochenodeoxycholic acid (GCDCA), glycodeoxycholic acid (GDCA) and deoxycholic acid (DCA), notable differences in passive diffusion were observed between the BAs tested upon addition of 500 pmol BA to the apical chamber, especially between the conjugated and unconjugated BAs. DCA was translocated primarily via passive diffusion, while for the conjugated BAs GCDCA and GDCA a very small amount (<LOQ) and for GCA no detectable amount was transported via passive diffusion. In line with literature, the passive BA diffusion rate followed their lipophilicity: DCA > GCDCA ≈ GDCA > GCA (Aldini et al., 1996).

Caco-2 cells are a robust intestinal cell model with apical brush borders, tight junctions and expression of several clinically relevant transporters, including transporters of the ATP binding cassette (ABC), multidrug resistance protein (MRP) and solute carrier (SLC) family (Olander et al., 2016; Antunes et al., 2013). Our results confirm that the GCA transport over Caco-2 cells is active and sodium-dependent, indicating the presence of a functional SLC-transporter. We trust that the Caco-2 cells performed ASBT-mediated BA transport, because a) GCA transport was completely inhibited upon addition of ≥0.5 nM of the selective ASBT inhibitor ODE at a low (5 µM) GCA concentration and b) our $K_{m,app}$ is within a 2-fold range of the $K_{m,app}$ value obtained from ASBT transfected MDCK cells reported in literature (Balakrishnan et al., 2006). Even though ASBT gene expression was confirmed for Caco-2 cells (Wang et al., 2022; van der Mark et al., 2014), ASBT protein expression was not conclusively demonstrated. ASBT protein expression could not be detected by LC-MS/MS (Bruck et al., 2017; Olander et al., 2016), but Western blot analysis by van der Mark et al. (2014) revealed that ASBT expression is low in Caco-2 cells compared to the human ileum. Differences in the detection limit of the analytical techniques, Caco-2 cell clones and/or culture conditions provide plausible explanations for the inconsistent results for ASBT protein expression in Caco-2 cells (Sambuy et al., 2005). We consider the sodium-dependency and ODE-mediated inhibition of GCA transport strong indicators of the presence of functional ASBT in Caco-2 monolayers. In the current study, an empirical scalar of 2.8 was employed to correct for differences between the *in vitro* and *in vivo* situation, such as differences in ASBT expression and/or activity and other chemical, physical, or biological differences. However, for optimal scientific validity, a mechanistic justification for the scaling factor is desirable, enabling its application to other substances. The mechanistic justification of the scaling factor could be based on the establishment of a relative activity factor (RAF), in which transport of a probe substrate *in vitro* is compared against the *in vivo* situation. RAFs have been proven relatively successful for the prediction of metabolic conversions, but their applicability for transporter-mediated processes remains to be verified (Kumar et al., 2021).

The Caco-2 cells were cultured in medium containing fetal calf serum (FCS). FCS contains an undefined cocktail of growth factors, hormones, vitamins and is typically used to ensure growth and proliferation in cell cultures. In order to contribute to the 3R (reduce, refine, replace) principles, increasing attention goes to the development of animal-free chemically-defined alternatives for FCS. Several synthetic supplements have been tested but did not allow various cell types to proliferate and differentiate properly (van der Valk et al., 2018). Human platelet lysate seems a promising substitute for FCS. Caco-2 cell viability was slightly enhanced in cells grown with this lysate compared to FCS, and the cells differentiated to cells of the enterocytic lineage (Wanes et al., 2021). Yet, functional similarity to the human intestinal epithelium remains to be demonstrated.

The kinetic parameters obtained in the Caco-2 transport assay were incorporated in a PBK model describing the synthesis, distribution, metabolism, and excretion of BAs. Our simulations for GCA, GDCA, and uBA accurately predicted the at least one dataset of observed BA concentrations, that is, within 2-fold. GCDCA postprandial kinetics were simulated with three different K_m values for NTCP-mediated transport, where the lowest value (0.6 µM, Jani et al., 2018) gave a close fit with the *in vivo* data, while the highest value (10 µM, Notenboom et al., 2018) resulted in a ~5-fold overprediction. The large discrepancy between the two experimental datasets can be attributed to intersystem (transfected CHO versus HEK293 cells), biological and/or chemical differences. Given its large influence on the postprandial kinetics, it is crucial to establish reliable kinetic parameters for NTCP-mediated transport and understand the reasons for these discrepancies. The predicted BA concentrations were still within the range of C_{max} values reported in literature. Up to 22-fold differences in plasma BA C_{max} between individuals have been reported, which could be due to biological interindividual differences (Baier et al., 2019; Lamaziere et al., 2020; Steiner et al., 2011; Fiamoncini et al., 2016), while interstudy differences between individuals may also be due to technical differences. Due to these differences a PBK model predicted C_{max} may be more than 2-fold different from data reported for individual volunteers in literature.

Our simulations reflect a consistently delayed time to reach C_{max} (T_{max}) compared to the *in vivo* datasets. The sensitivity analysis revealed that a prolonged gall bladder ejection time had the strongest delaying effect on T_{max}. In the current model the gall bladder ejection time was set to 90 minutes, which was derived from a study using scintigraphy measurements in healthy individuals. In this study, the volunteers were administered an isotope and the isotope amount in the gallbladder was

quantified at selected timepoints using a gamma camera (Jazrawi et al., 1995). The accuracy of the predicted T_{max} might be improved by describing gall bladder motility in more detail, for example by using a normalized Rayleigh function which shows a transient increase and subsequent decrease of gall bladder emptying rate over time (Sips et al., 2018). Given that the effect of gall bladder ejection time on T_{max} was relatively small (NSC<0.1), this approach was not applied in the current work.

The data from our transport assays indicated that ODE is a competitive inhibitor of GCA transport, with an estimated IC_{50} of 0.04 nM which is about 2-fold lower than literature (0.1 nM) (EMA, 2021). We predicted a decrease in plasma BAs, and especially the conjugated BAs (GCA, GCDCA and GDCA), upon treatment with a single oral dose of ODE. The decrease in total BAs was in line with literature. *In vivo* data in healthy individuals on day 7 of treatment with ODE showed a similar change in BA profile, i.e., a decrease in plasma conjugated BAs and a slight increase in the unconjugated BAs DCA and CDCA (Graffner et al., 2016). The authors also observed an increase in fecal unconjugated BAs on day 7 of ODE treatment. Likewise, we simulated an increased amount of colonic unconjugated BAs, which can be directly translated into increased fecal amounts due to reduced intestinal ASBT mediated uptake of these conjugated BAs. Treatment with 3 mg ODE is shown to significantly reduce plasma fibroblast growth factor 19 (FGF-19) levels in healthy individuals. This results in a reduced inhibition of hepatic BA synthesis, which is reflected by increased plasma levels of the BA precursor C4 (Graffner et al., 2016). It is important to note that the PBK model developed included only a basic adaptive response, which does not allow for dynamic changes in synthesis rate, microbiome's composition or intestinal membrane integrity. Therefore, we only modeled the effects of ODE upon a single administration. Quantitatively capturing dynamic changes in a computational model requires many assumptions and fitting of parameters, which has been done previously (Voronova et al., 2020). A major strength of our PBK model is that the majority of input parameters is derived experimentally, but accordingly the adaptive response was not modelled in detail. Nevertheless, the current model is proven useful for the prediction of short-term effects in healthy individuals.

In the current work, we report an apparent Michaelis Menten constant or $K_{m,app}$, because the value relates to the overall process of transport across the Caco-2 monolayer including not only apical influx, but also intracellular transport by bile acid binding protein (BABP) and basolateral efflux by organic solute transporter (OST) α/β. The $K_{m,app}$ can differ between *in vitro* and *in vivo* test systems. For example, for taurocholic acid (TCA), the typical model BA for transport experiments, $K_{m,app}$ values for intestinal uptake ranging from 4.4 to 600 µM have been reported using transfected cell lines/oocytes, human precision cut intestinal slices and a human perfusion study *in vivo* (Balakrishnan et al., 2006; Zhu et al., 2021; Li et al., 2018; Krag and Phillips, 1974). Besides biological differences in e.g., OSTα/β or BABP activity, the physical hydrodynamic barrier between the bulk solution and the surface with the transporter differs depending on the test system used. *In vitro* the restricted liquid flow in the vicinity of a culture insert will create a zone where the diffusional movement of molecules exceeds the convection. The formed layer is referred to as the unstirred water layer or aqueous boundary layer (ABL). Besides, the culture insert itself will affect the compound's permeability (Korjamo et al., 2009). Balakrishnan et al. (2007) studied the effect of the ABL in culture inserts and derived an equation that can be used to correct the affinity of influx transporters for the ABL. This equation was employed in this work (Eq. 2), and resulted in a $K_{m,app}$ of 23 µM, versus 39 µM when the resistance by the ABL was not considered. The intestinal peristaltic movements can be expected to drastically reduce the ABL *in vivo* resulting in lower $K_{m,app}$ values. It has been concluded previously that the ABL does not play a clinically significant role in the intestinal absorption of drugs *in vivo* and hence, $K_{m,app}$ values derived from static *in vitro* models should be corrected for the ABL before the values can be extrapolated to the *in vivo* situation (Korjamo et al., 2009). Where *in vitro* the ABL hampers a molecule's transport to a culture insert, *in vivo* a molecule first has to migrate through the mucus layer before it reaches the intestinal epithelium. Caco-2 cells represent cells of the enterocytic lineage, and do not fully represent the cell types present in the human ileal epithelium. Especially the lack of mucin-producing Goblet cells and thus a mucus layer could affect the $K_{m,app}$. The HT29-MTX cell line has emerged as a cell line that forms Goblet cells and can be used to complement Caco-2 cells. Co-culturing HT29-MTX cells with Caco-2 cells results in similar gene expression profiles to gastrointestinal tissue, and a mucus layer on top of the epithelium (Pontier et al., 2001). Yet, coculturing HT29-MTX and Caco-2 cells did not modulate permeability compared to Caco-2 cells alone, and ergo does not provide an improved $K_{m,app}$ that takes into account the mucus effects (McCright et al., 2022; Lock et al., 2018). Due to the absence of functional differences in permeability between the coculture and monoculture system, we have decided to use the well-characterized and robust Caco-2 monoculture system.

The current results underline the importance of active ileal and hepatic transport processes for accurate predictions of systemic plasma BA levels. We demonstrate that Caco-2 cells can be used to quantitatively study ODE's inhibitory effects on GCA transport. By incorporating the obtained kinetic parameters in a PBK model we were able to accurately predict the changes in plasma BA levels upon a single oral dose of ODE. The current model can serve as a quantitative tool to predict alterations in plasma BA levels upon xenobiotic-exposure.

References

Al-Hilal, T. A., Chung, S. W., Alam, F. et al. (2014). Functional transformations of bile acid transporters induced by high-affinity macromolecules. *Sci Rep 4*, 4163. doi:10.1038/srep04163

Aldini, R., Roda, A., Montagnani, M. et al. (1996). Relationship between structure and intestinal absorption of bile acids with a steroid or side-chain modification. *Steroids 61*, 590-597. doi:10.1016/s0039-128x(96)00119-5

Antunes, F., Andrade, F., Araujo, F. et al. (2013). Establishment of a triple co-culture in vitro cell models to study intestinal absorption of peptide drugs. *Eur J Pharm Biopharm 83*, 427-435. doi:10.1016/j.ejpb.2012.10.003

Baier, V., Cordes, H., Thiel, C. et al. (2019). A physiology-based model of human bile acid metabolism for predicting bile acid tissue levels after drug administration in healthy subjects and bric type 2 patients. *Front Physiol 10*, 1192. doi:10.3389/fphys.2019.01192

Balakrishnan, A., Wring, S. A. and Polli, J. E. (2006). Interaction of native bile acids with human apical sodium-dependent bile acid transporter (hasbt): Influence of steroidal hydroxylation pattern and c-24 conjugation. *Pharm Res 23*, 1451-1459. doi:10.1007/s11095-006-0219-4

Balakrishnan, A., Hussainzada, N., Gonzalez, P. et al. (2007). Bias in estimation of transporter kinetic parameters from overexpression systems: Interplay of transporter expression level and substrate affinity. *J Pharmacol Exp Ther 320*, 133-144. doi:10.1124/jpet.106.107433

Barter, Z. E., Bayliss, M. K., Beaune, P. H. et al. (2007). Scaling factors for the extrapolation of in vivo metabolic drug clearance from in vitro data: Reaching a consensus on values of human micro-somal protein and hepatocellularity per gram of liver. *Current drug metabolism 8*, 33-45. doi:10.2174/138920007779315053

Bathena, S. P. R., Mukherjee, S., Olivera, M. et al. (2013). The profile of bile acids and their sulfate metabolites in human urine and serum. *Journal of Chromatography B-Analytical Technologies in the Biomedical and Life Sciences 942*, 53-62. doi:10.1016/j.jchromb.2013.10.019

Begley, M., Gahan, C. G. M. and Hill, C. (2005). The interaction between bacteria and bile. *Fems Microbiology Reviews 29*, 625-651. doi:10.1016/j.femsre.2004.09.003

Bruck, S., Strohmeier, J., Busch, D. et al. (2017). Caco-2 cells - expression, regulation and function of drug transporters compared with human jejunal tissue. *Biopharm Drug Dispos 38*, 115-126. doi:10.1002/bdd.2025

Chiang, J. Y. and Ferrell, J. M. (2022). Discovery of farnesoid x receptor and its role in bile acid metabolism. *Molecular and Cellular Endocrinology* 111618. doi:10.1016/j.mce.2022.111618

Dawson, P. A., Lan, T. and Rao, A. (2009). Bile acid transporters. *Journal of lipid research 50*, 2340-2357.

Dawson, P. A. (2011). Role of the intestinal bile acid transporters in bile acid and drug disposition. *Handb Exp Pharmacol* 169-203. doi:10.1007/978-3-642-14541-4_4

de Bruijn, V. M. P., Rietjens, I. and Bouwmeester, H. (2022a). Population pharmacokinetic model to generate mechanistic insights in bile acid homeostasis and drug-induced cholestasis. *Arch Toxicol 96*, 2717-2730. doi:10.1007/s00204-022-03345-8

de Bruijn, V. M. P., Wang, Z., Bakker, W. et al. (2022b). Hepatic bile acid synthesis and secretion: Comparison of in vitro methods. *Toxicol Lett 365*, 46-60. doi:10.1016/j.toxlet.2022.06.004

Deeks, E. D. (2021). Odevixibat: First approval. *Drugs* 1-6. doi:10.1007/s40265-021-01594-y

Duan, S., Li, X., Fan, G. et al. (2022). Targeting bile acid signaling for the treatment of liver diseases: From bench to bed. *Biomed Pharmacother 152*, 113154. doi:10.1016/j.biopha.2022.113154

EMA - European Medicines Agency (2021). Assessment report: Bylvay. Committee for Medicinal Products for Human Use (CHMP). EMA/319560/2021 https://www.ema.europa.eu/en/documents/assessment-report/bylvay-epar-public-assessment-report_en.pdf

Evans, M. V. and Andersen, M. E. (2000). Sensitivity analysis of a physiological model for 2,3,7,8-tetrachlorodibenzo-p-dioxin (TCDD): assessing the impact of specific model parameters on sequestration in liver and fat in the rat. *Toxicol Sci 54*, 71-80. doi:10.1093/toxsci/54.1.71

Falany, C. N., Johnson, M. R., Barnes, S. et al. (1994). Glycine and taurine conjugation of bile acids by a single enzyme. Molecular cloning and expression of human liver bile acid coa:Amino acid n-acyltransferase. *J Biol Chem 269*, 19375-19379.

Fasano, A., Budillon, G., Guandalini, S. et al. (1990). Bile acids reversible effects on small intestinal permeability. An in vitro study in the rabbit. *Dig Dis Sci 35*, 801-808. doi:10.1007/BF01536791

Fiamoncini, J., Curi, R. and Daniel, H. (2016). Metabolism of bile acids in the post-prandial state. *Essays in biochemistry 60*, 409-418. doi:10.1042/EBC20160052

Fitzpatrick, L. R. and Jenabzadeh, P. (2020). Ibd and bile acid absorption: Focus on pre-clinical and clinical observations. *Front Physiol 11*, 564. doi:10.3389/fphys.2020.00564

Fuchs, C. D. and Trauner, M. (2022). Role of bile acids and their receptors in gastrointestinal and hepatic pathophysiology. *Nature Reviews Gastroenterology & Hepatology 19*, 432-450. doi:10.1038/s41575-021-00566-7

Garcia-Canaveras, J. C., Donato, M. T., Castell, J. V. et al. (2012). Targeted profiling of circulating and hepatic bile acids in human, mouse, and rat using a uplc-mrm-ms-validated method. *J Lipid Res 53*, 2231-2241. doi:10.1194/jlr.D028803

Gijbels, E. and Vinken, M. (2019). Mechanisms of drug-induced cholestasis. In (eds.), *Experimental cholestasis research*. Springer.

Gilbert-Sandoval, I., Wesseling, S. and Rietjens, I. (2020). Predicting the acute liver toxicity of aflatoxin b1 in rats and humans by an in vitro-in silico testing strategy. *Mol Nutr Food Res 64*, e2000063. doi:10.1002/mnfr.202000063

Graffner, H., Gillberg, P. G., Rikner, L. et al. (2016). The ileal bile acid transporter inhibitor a4250 decreases serum bile acids by interrupting the enterohepatic circulation. *Aliment Pharmacol Ther 43*, 303-310. doi:10.1111/apt.13457

Hendriksen, B. A., Felix, M. V. and Bolger, M. B. (2003). The composite solubility versus ph profile and its role in intestinal absorption prediction. *AAPS PharmSci 5*, E4. doi:10.1208/050104

Hepner, G. W. and Demers, L. M. (1977). Dynamics of the enterohepatic circulation of the glycine conjugates of cholic, chenodeoxycholic, deoxycholic, and sulfolithocholic acid in man. *Gastroenterology 72*, 499-501.

Hofmann, A. F., Molino, G., Milanese, M. et al. (1983). Description and simulation of a physiological pharmacokinetic model for the metabolism and enterohepatic circulation of bile acids in man. Cholic acid in healthy man. *J Clin Invest 71*, 1003-1022. doi:10.1172/jci110828

Jamei, M., Bajot, F., Neuhoff, S. et al. (2014). A mechanistic framework for in vitro–in vivo extrapolation of liver membrane transporters: Prediction of drug–drug interaction between rosuvastatin and cyclosporine. *Clinical pharmacokinetics 53*, 73-87. doi:10.1007/s40262-013-0097-y

Jani, M., Beéry, E., Heslop, T. et al. (2018). Kinetic characterization of bile salt transport by human ntcp (slc10a1). *Toxicology in Vitro 46*, 189-193. doi:10.1016/j.tiv.2017.10.012

Jazrawi, R. P., Pazzi, P., Petroni, M. L. et al. (1995). Postprandial gallbladder motor function: Refilling and turnover of bile in health and in cholelithiasis. *Gastroenterology 109*, 582-591. doi:10.1016/0016-5085(95)90348-8

Jia, W., Xie, G. and Jia, W. (2018). Bile acid-microbiota crosstalk in gastrointestinal inflammation and carcinogenesis. *Nat Rev Gastroenterol Hepatol 15*, 111-128. doi:10.1038/nrgastro.2017.119

Kararli, T. T. (1995). Comparison of the gastrointestinal anatomy, physiology, and biochemistry of humans and commonly used laboratory animals. *Biopharm Drug Dispos 16*, 351-380. doi:10.1002/bdd.2510160502

Kato, T., Mikami, Y., Sun, L. et al. (2021). Reuse of cell culture inserts for in vitro human primary airway epithelial cell studies. *Am J Respir Cell Mol Biol 64*, 760-764. doi:10.1165/rcmb.2021-0033LE

Kimura, T. and Higaki, K. (2002). Gastrointestinal transit and drug absorption. *Biol Pharm Bull 25*, 149-164. doi:10.1248/bpb.25.149

Kis, E., Ioja, E., Nagy, T. et al. (2009). Effect of membrane cholesterol on bsep/bsep activity: Species specificity studies for substrates and inhibitors. *Drug Metab Dispos 37*, 1878-1886. doi:10.1124/dmd.108.024778

Korjamo, T., Heikkinen, A. T. and Monkkonen, J. (2009). Analysis of unstirred water layer in in vitro permeability experiments. *J Pharm Sci 98*, 4469-4479. doi:10.1002/jps.21762

Kouzuki, H., Suzuki, H., Ito, K. et al. (1998). Contribution of sodium taurocholate co-transporting polypeptide to the uptake of its possible substrates into rat hepatocytes. *Journal of Pharmacology and Experimental Therapeutics 286*, 1043-1050.

Krag, E. and Phillips, S. F. (1974). Active and passive bile acid absorption in man. Perfusion studies of the ileum and jejunum. *J Clin Invest 53*, 1686-1694. doi:10.1172/JCI107720

Kullak-Ublick, G. A., Stieger, B. and Meier, P. J. (2004). Enterohepatic bile salt transporters in normal physiology and liver disease. *Gastroenterology 126*, 322-342. doi:10.1053/j.gastro.2003.06.005

Kumar, A. R., Prasad, B., Bhatt, D. K. et al. (2021). In vitro–to–in vivo extrapolation of transporter-mediated renal clearance: Relative expression factor versus relative activity factor approach. *Drug Metabolism and Disposition 49*, 470-478. doi:10.1124/dmd.121.000367

Lamaziere, A., Rainteau, D., Kc, P. et al. (2020). Distinct postprandial bile acids responses to a high-calorie diet in men volunteers underscore metabolically healthy and unhealthy phenotypes. *Nutrients 12*, 3545. doi:10.3390/nu12113545

Law, V., Knox, C., Djoumbou, Y. et al. (2014). Drugbank 4.0: Shedding new light on drug metabolism. *Nucleic Acids Res 42*, D1091-1097. doi:10.1093/nar/gkt1068

Leschelle, X., Robert, V., Delpal, S. et al. (2002). Isolation of pig colonic crypts for cytotoxic assay of luminal compounds: Effects of hydrogen sulfide, ammonia, and deoxycholic acid. *Cell Biol Toxicol 18*, 193-203. doi:10.1023/a:1015515821390

Li, M., Vokral, I., Evers, B. et al. (2018). Human and rat precision-cut intestinal slices as ex vivo models to study bile acid uptake by the apical sodium-dependent bile acid transporter. *European Journal of Pharmaceutical Sciences 121*, 65-73. doi:10.1016/j.ejps.2018.05.005

Li, S., Qu, X., Zhang, L. et al. (2022). Serum total bile acids in relation to gastrointestinal cancer risk: A retrospective study. *Front Oncol 12*, 859716. doi:10.3389/fonc.2022.859716

Lin, S., Wang, S., Wang, P. et al. (2023). Bile acids and their receptors in regulation of gut health and diseases. *Prog Lipid Res 89*, 101210. doi:10.1016/j.plipres.2022.101210

Lineweaver, H. and Burk, D. (1934). The determination of enzyme dissociation constants. *Journal of the American chemical society 56*, 658-666.

Lobell, M. and Sivarajah, V. (2003). In silico prediction of aqueous solubility, human plasma protein binding and volume of distribution of compounds from calculated pk(a) and alogp98 values. *Molecular Diversity 7*, 69-87. doi:10.1023/b:modi.0000006562.93049.36

Lock, J. Y., Carlson, T. L. and Carrier, R. L. (2018). Mucus models to evaluate the diffusion of drugs and particles. *Adv Drug Deliv Rev 124*, 34-49. doi:10.1016/j.addr.2017.11.001

Lu, Z. N., He, H. W. and Zhang, N. (2022). Advances in understanding the regulatory mechanism of organic solute transporter alpha-beta. *Life Sci 310*, 121109. doi:10.1016/j.lfs.2022.121109

Marasco, G., Cremon, C., Barbaro, M. R. et al. (2022). Pathophysiology and clinical management of bile acid diarrhea. *J Clin Med 11*, 3102. doi:10.3390/jcm11113102

Martinez-Augustin, O. and Sanchez de Medina, F. (2008). Intestinal bile acid physiology and pathophysiology. *World J Gastroenterol 14*, 5630-5640. doi:10.3748/wjg.14.5630

McCright, J., Sinha, A. and Maisel, K. (2022). Generating an in vitro gut model with physiologically relevant biophysical mucus properties. *Cell Mol Bioeng 15*, 479-491. doi:10.1007/s12195-022-00740-0

Miele, L., Valenza, V., La Torre, G. et al. (2009). Increased intestinal permeability and tight junction alterations in nonalcoholic fatty liver disease. *Hepatology 49*, 1877-1887. doi:10.1002/hep.22848

Molino, G., Hofmann, A. F., Cravetto, C. et al. (1986). Simulation of the metabolism and enterohepatic circulation of endogenous chenodeoxycholic acid in man using a physiological pharmacokinetic model. *Eur J Clin Invest 16*, 397-414. doi:10.1111/j.1365-2362.1986.tb01015.x

Mouzaki, M., Wang, A. Y., Bandsma, R. et al. (2016). Bile acids and dysbiosis in non-alcoholic fatty liver disease. *PLoS One 11*, e0151829. doi:10.1371/journal.pone.0151829

Notenboom, S., Weigand, K. M., Proost, J. H. et al. (2018). Development of a mechanistic biokinetic model for hepatic bile acid handling to predict possible cholestatic effects of drugs. *European Journal of Pharmaceutical Sciences 115*, 175-184. doi:10.1016/j.ejps.2018.01.007

Olander, M., Wisniewski, J. R., Matsson, P. et al. (2016). The proteome of filter-grown caco-2 cells with a focus on proteins involved in drug disposition. *J Pharm Sci 105*, 817-827. doi:10.1016/j.xphs.2015.10.030

Peyret, T., Poulin, P. and Krishnan, K. (2010). A unified algorithm for predicting partition coefficients for pbpk modeling of drugs and environmental chemicals. *Toxicology and applied pharmacology 249*, 197-207. doi:10.1016/j.taap.2010.09.010

Pontier, C., Pachot, J., Botham, R. et al. (2001). Ht29-mtx and caco-2/tc7 monolayers as predictive models for human intestinal absorption: Role of the mucus layer. *Journal of Pharmaceutical Sciences 90*, 1608-1619. doi:10.1002/jps.1111

Punt, A., Pinckaers, N., Peijnenburg, A. et al. (2020). Development of a web-based toolbox to support quantitative in-vitro-to-in-vivo extrapolations (qivive) within nonanimal testing strategies. *Cheml Res Toxicol 34*, 460-472. doi:10.1021/acs.chemrestox.0c00307

Punt, A., Louisse, J., Beekmann, K. et al. (2022). Predictive performance of next generation human physiologically based kinetic (pbk) models based on in vitro and in silico input data. *ALTEX 39*, 221-234. doi:10.14573/altex.2108301

Rietjens, I. M., Louisse, J. and Punt, A. (2011). Tutorial on physiologically based kinetic modeling in molecular nutrition and food research. *Molecular nutrition & food research 55*, 941-956. doi:10.1002/mnfr.201000655

Ritz, C., Baty, F., Streibig, J. C. et al. (2015). Dose-response analysis using r. *PLoS One 10*, e0146021. doi:10.1371/journal.pone.0146021

Roda, A., Minutello, A., Angellotti, M. A. et al. (1990). Bile acid structure-activity relationship: Evaluation of bile acid lipophilicity using 1-octanol/water partition coefficient and reverse phase hplc. *J Lipid Res 31*, 1433-1443.

Rodgers, T. and Rowland, M. (2006). Physiologically based pharmacokinetic modelling 2: Predicting the tissue distribution of acids, very weak bases, neutrals and zwitterions. *Journal of Pharmaceutical Sciences 95*, 1238-1257. doi:10.1002/jps.20502

Sabino, J., Vieira-Silva, S., Machiels, K. et al. (2016). Primary sclerosing cholangitis is characterised by intestinal dysbiosis independent from ibd. *Gut 65*, 1681-1689. doi:10.1136/gutjnl-2015-311004

Sambuy, Y., Angelis, I., Ranaldi, G. et al. (2005). The caco-2 cell line as a model of the intestinal barrier: Influence of cell and culture-related factors on caco-2 cell functional characteristics. *Cell Biology and Toxicology 21*, 1-26. doi:10.1007/s10565-005-0085-6

Schwarz, M. A., Neubert, R. H. and Rüttinger, H. H. (1996). Application of capillary electrophoresis for characterizing interactions between drugs and bile salts. Part i. *Journal of Chromatography A 745*, 135-143.

Sharanek, A., Burban, A., Humbert, L. et al. (2015). Cellular accumulation and toxic effects of bile acids in cyclosporine a-treated heparg hepatocytes. *Toxicological Sciences 147*, 573-587. doi:10.1093/toxsci/kfv155

Shrivastava, A. and Gupta, V. B. (2011). Methods for the determination of limit of detection and limit of quantitation of the analytical methods. *Chron. Young Sci 2*, 21-25.

Sips, F. L. P., Eggink, H. M., Hilbers, P. A. J. et al. (2018). In silico analysis identifies intestinal transit as a key determinant of systemic bile acid metabolism. *Front Physiol 9*, 631. doi:10.3389/fphys.2018.00631

Smirnova, E., Muthiah, M. D., Narayan, N. et al. (2022). Metabolic reprogramming of the intestinal microbiome with functional bile acid changes underlie the development of nafld. *Hepatology 76*, 1811-1824. doi:10.1002/hep.32568

Soars, M., Burchell, B. and Riley, R. (2002). In vitro analysis of human drug glucuronidation and prediction of in vivo metabolic clearance. *Journal of Pharmacology and Experimental Therapeutics 301*, 382-390. doi:10.1124/jpet.301.1.382

Soetaert, K. and Petzoldt, T. (2010). Inverse modelling, sensitivity and monte carlo analysis in r using package fme. *Journal of Statistical Software 33*, 1-28. doi:10.18637/jss.v033.i03

Steiner, C., Othman, A., Saely, C. H. et al. (2011). Bile acid metabolites in serum: Intraindividual variation and associations with coronary heart disease, metabolic syndrome and diabetes mellitus. *PLOS ONE 6*, e25006. doi:10.1371/journal.pone.0025006

Toke, O. (2022). Structural and dynamic determinants of molecular recognition in bile acid-binding proteins. *International Journal of Molecular Sciences 23*, 505. doi:10.3390/ijms23010505

van der Mark, V. A., de Waart, D. R., Ho-Mok, K. S. et al. (2014). The lipid flippase heterodimer atp8b1–cdc50a is essential for surface expression of the apical sodium-dependent bile acid transporter (slc10a2/asbt) in intestinal caco-2 cells. *Biochimica et Biophysica Acta (BBA)-Molecular Basis of Disease 1842*, 2378-2386. doi:10.1016/j.bbadis.2014.09.003

van der Valk, J., Bieback, K., Buta, C. et al. (2018). Fetal bovine serum (fbs): Past - present - future. *ALTEX 35*, 99-118. doi:10.14573/altex.1705101

Vinken, M., Landesmann, B., Goumenou, M. et al. (2013). Development of an adverse outcome pathway from drug-mediated bile salt export pump inhibition to cholestatic liver injury. *Toxicol Sci 136*, 97-106. doi:10.1093/toxsci/kft177

Voronova, V., Sokolov, V., Al-Khaifi, A. et al. (2020). A physiology-based model of bile acid distribution and metabolism under healthy and pathologic conditions in human beings. *Cell Mol Gastroenterol Hepatol 10*, 149-170. doi:10.1016/j.jcmgh.2020.02.005

Wanes, D., Naim, H. Y. and Dengler, F. (2021). Proliferation and differentiation of intestinal caco-2 cells are maintained in culture with human platelet lysate instead of fetal calf serum. *Cells 10*, 3038. doi:10.3390/cells10113038

Wang, J., Bakker, W., Zheng, W. et al. (2022). Exposure to the mycotoxin deoxynivalenol reduces the transport of conjugated bile acids by intestinal caco-2 cells. *Arch Toxicol 96*, 1473-1482. doi:10.1007/s00204-022-03256-8

Wang, Q., Strab, R., Kardos, P. et al. (2008). Application and limitation of inhibitors in drug-transporter interactions studies. *Int J Pharm 356*, 12-18. doi:10.1016/j.ijpharm.2007.12.024

Yang, N., Dong, Y. Q., Jia, G. X. et al. (2020). Asbt(slc10a2): A promising target for treatment of diseases and drug discovery. *Biomed Pharmacother 132*, 110835. doi:10.1016/j.biopha.2020.110835

Zhang, N., Wang, J., Bakker, W. et al. (2022). In vitro models to detect in vivo bile acid changes induced by antibiotics. *Arch Toxicol 96*, 3291-3303. doi:10.1007/s00204-022-03373-4

Zhu, Q., Komori, H., Imamura, R. et al. (2021). A novel fluorescence-based method to evaluate ileal apical sodium-dependent bile acid transporter asbt. *J Pharm Sci 110*, 1392-1400. doi:10.1016/j.xphs.2020.11.030

Data availability

The model code can be found in the supplementary file[1]. The input parameters are provided in .xlsx format in the supplementary file[5]. In *vitro* transport data are available upon request from the corresponding author.

Conflict of interest

The authors do not report a conflict of interest.

Acknowledgements

We would like to thank Wouter Bakker for his help with the LC-MS/MS measurements.